Neuron

Supplemental Information

Congenital Nystagmus Gene FRMD7 Is Necessary for Establishing a Neuronal Circuit Asymmetry for Direction Selectivity

Keisuke Yonehara, Michele Fiscella, Antonia Drinnenberg, Federico Esposti, Stuart Trenholm, Jacek Krol, Felix Franke, Brigitte Gross Scherf, Akos Kusnyerik, Jan Müller, Arnold Szabo, Josephine Jüttner, Francisco Cordoba, Ashrithpal Police Reddy, János Németh, Zoltán Zsolt Nagy, Francis Munier, Andreas Hierlemann, and Botond Roska

Figure S1

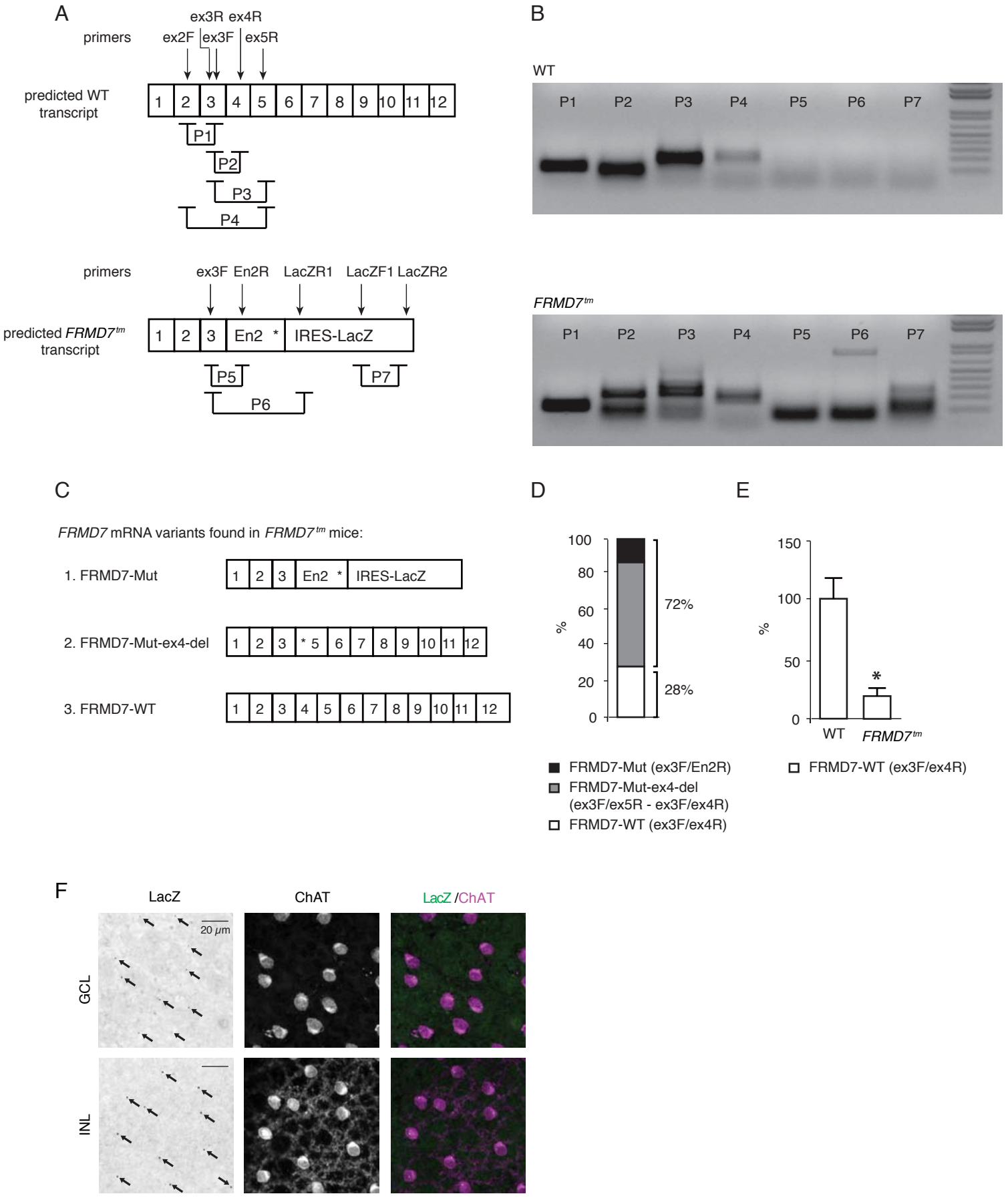
A
primers
ex3R ex4R
ex2F ex3F ex5R
predicted WT transcript
1 2 3 4 5 6 7 8 9 10 11 12
P1
P2
P3
P4
primers
ex3F En2R LacZR1 LacZF1 LacZR2
predicted FRMD7tm transcript
1 2 3 En2 * IRES-LacZ
P5
P7
P6
B
WT
P1 P2 P3 P4 P5 P6 P7
FRMD7tm
P1 P2 P3 P4 P5 P6 P7
C
FRMD7 mRNA variants found in FRMD7tm mice:
1. FRMD7-Mut
1 2 3 En2 * IRES-LacZ
2. FRMD7-Mut-ex4-del
1 2 3 * 5 6 7 8 9 10 11 12
3. FRMD7-WT
1 2 3 4 5 6 7 8 9 10 11 12
D
100
80
60
40
20
0
%
72%
28%
FRMD7-Mut (ex3F/En2R)
FRMD7-Mut-ex4-del (ex3F/ex5R - ex3F/ex4R)
FRMD7-WT (ex3F/ex4R)
E
150
100
50
0
%
*
WT
FRMD7tm
FRMD7-WT (ex3F/ex4R)
F
LacZ
ChAT
LacZ /ChAT
20 μm
GCL
INL

Figure S2

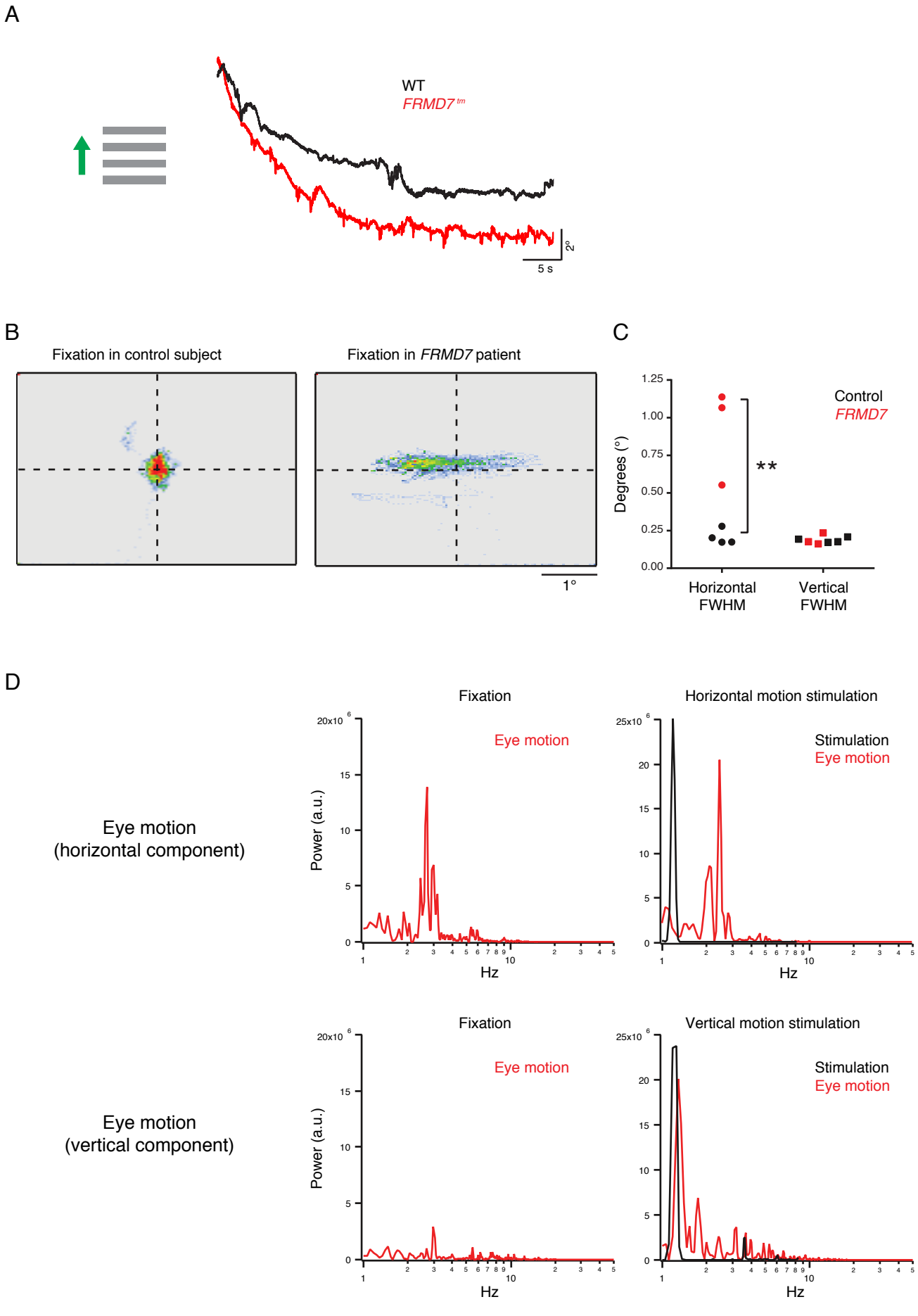
A
WT
FRMD7 tm
2°
5 s
B
Fixation in control subject
Fixation in FRMD7 patient
1°
C
Control
FRMD7
Degrees (°)
1.25
1.00
0.75
0.50
0.25
0.00
**
Horizontal FWHM
Vertical FWHM
D
Eye motion (horizontal component)
Fixation
Horizontal motion stimulation
Eye motion
Stimulation
Eye motion
Power (a.u.)
Hz
Eye motion (vertical component)
Fixation
Vertical motion stimulation
Eye motion
Stimulation
Eye motion
Power (a.u.)
Hz

Figure S3

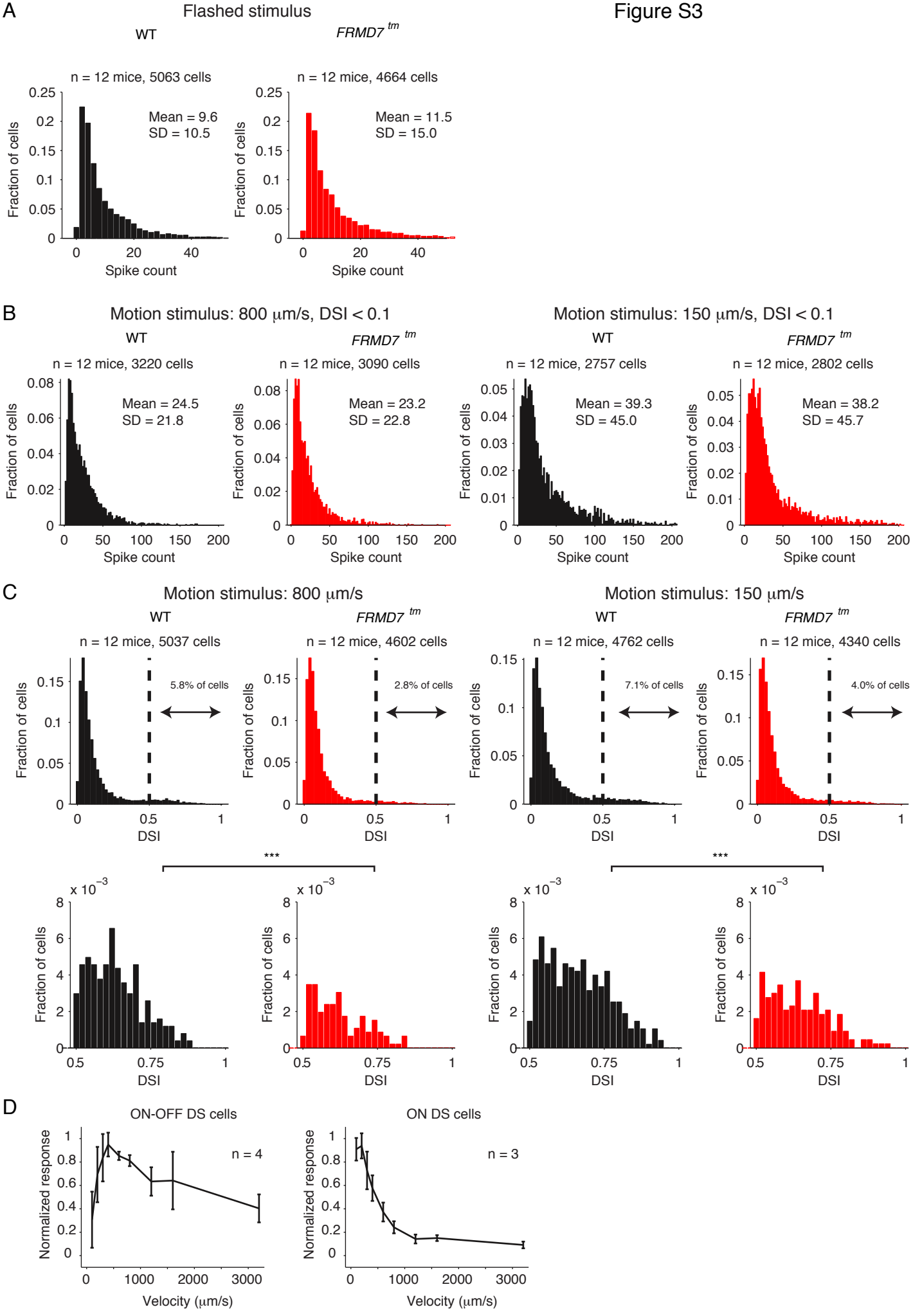
A
Flashed stimulus
WT
FRMD7 tm
n = 12 mice, 5063 cells
Mean = 9.6
SD = 10.5
n = 12 mice, 4664 cells
Mean = 11.5
SD = 15.0
Fraction of cells
Spike count
B
Motion stimulus: 800 μm/s, DSI < 0.1
Motion stimulus: 150 μm/s, DSI < 0.1
n = 12 mice, 3220 cells
Mean = 24.5
SD = 21.8
n = 12 mice, 3090 cells
Mean = 23.2
SD = 22.8
n = 12 mice, 2757 cells
Mean = 39.3
SD = 45.0
n = 12 mice, 2802 cells
Mean = 38.2
SD = 45.7
C
Motion stimulus: 800 μm/s
Motion stimulus: 150 μm/s
n = 12 mice, 5037 cells
5.8% of cells
n = 12 mice, 4602 cells
2.8% of cells
n = 12 mice, 4762 cells
7.1% of cells
n = 12 mice, 4340 cells
4.0% of cells
DSI
***
x 10−3
D
ON-OFF DS cells
n = 4
ON DS cells
n = 3
Normalized response
Velocity (μm/s)

Figure S4

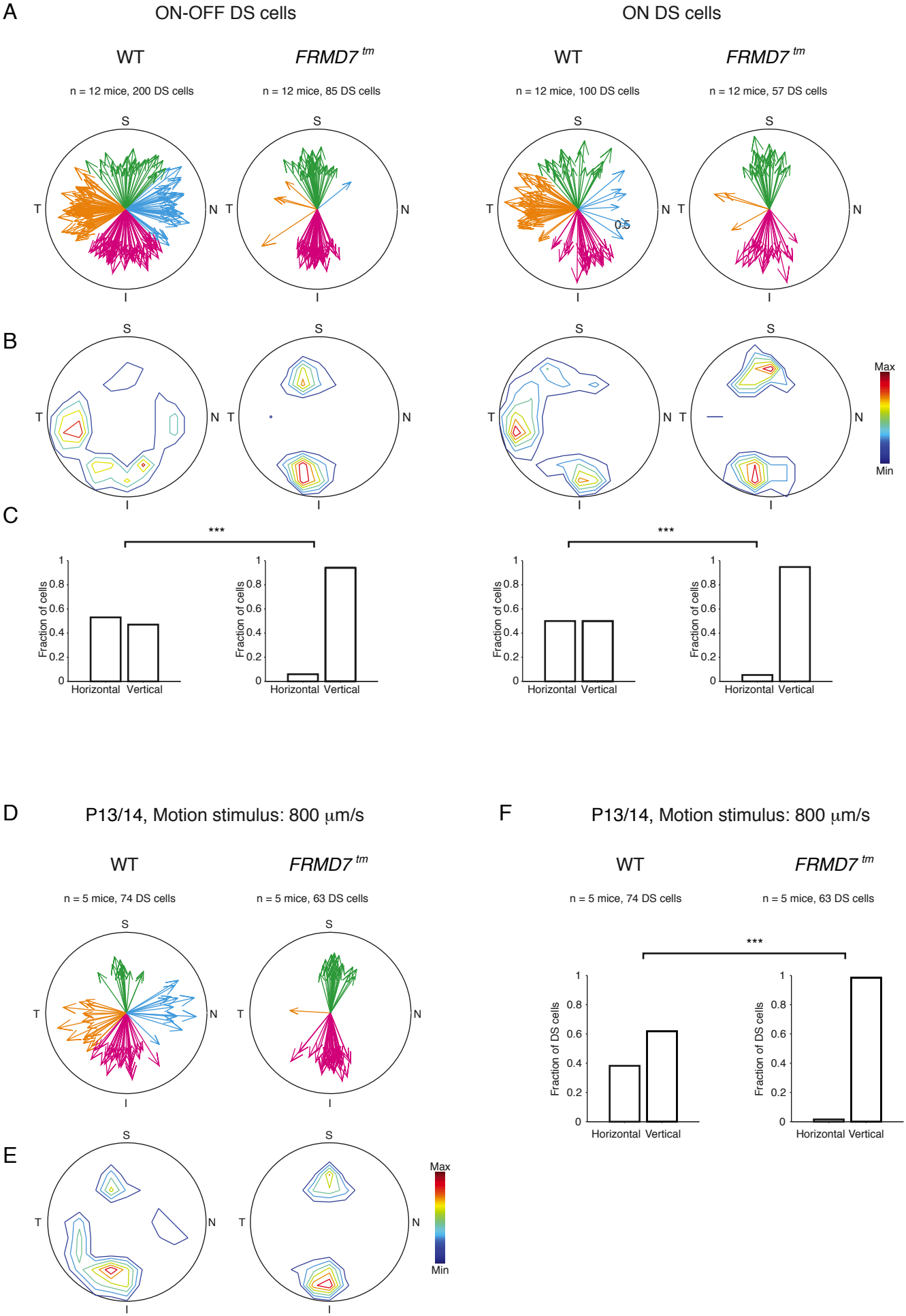
A
ON-OFF DS cells
ON DS cells
WT
FRMD7 tm
n = 12 mice, 200 DS cells
n = 12 mice, 85 DS cells
n = 12 mice, 100 DS cells
n = 12 mice, 57 DS cells
S
T
N
I
0.5
B
Max
Min
C
***
Fraction of cells
Horizontal
Vertical
D
P13/14, Motion stimulus: 800 μm/s
n = 5 mice, 74 DS cells
n = 5 mice, 63 DS cells
E
F
Fraction of DS cells

Figure S5

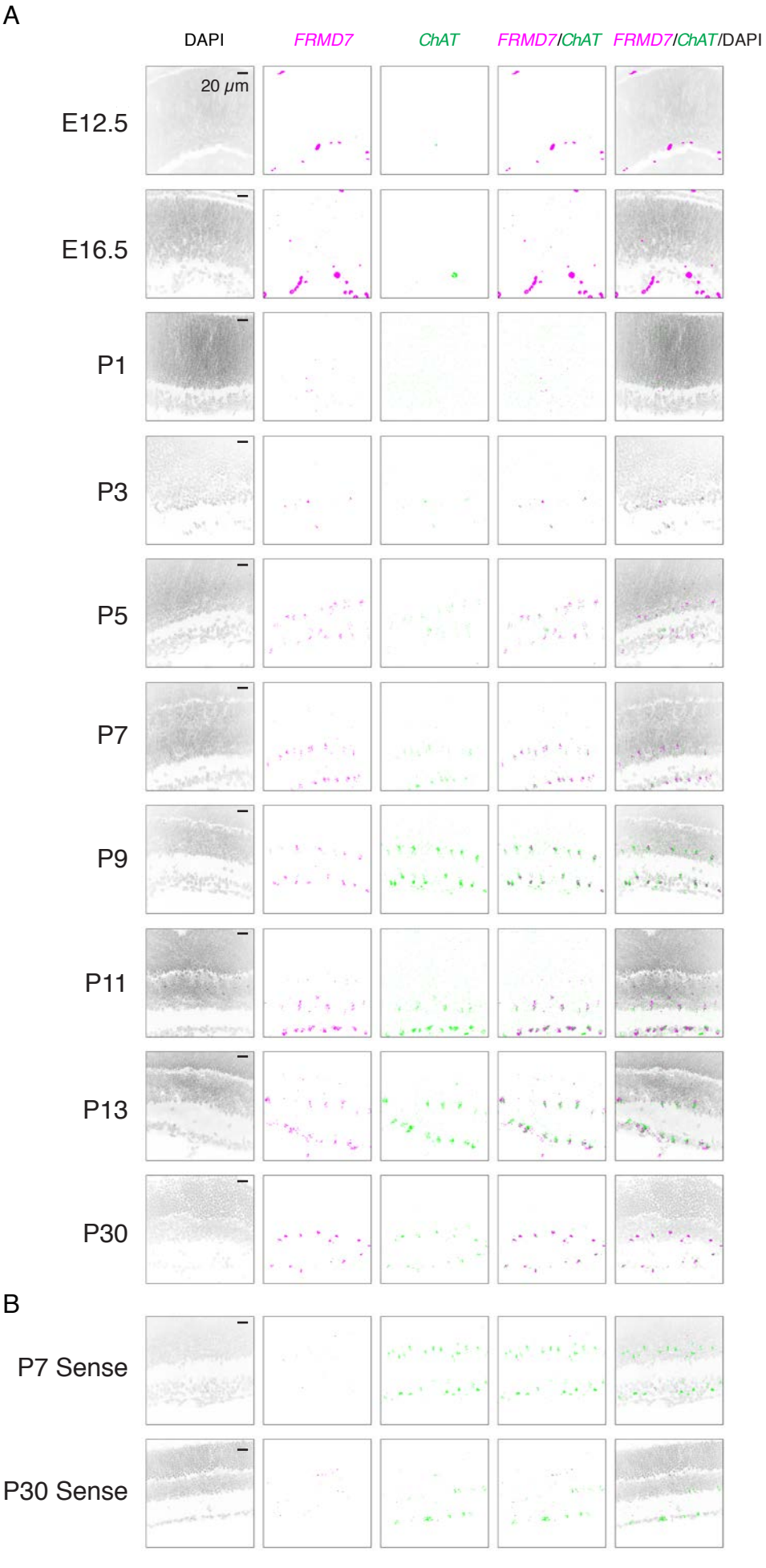
A
DAPI
FRMD7
ChAT
FRMD7/ChAT
FRMD7/ChAT/DAPI
20 μm
E12.5
E16.5
P1
P3
P5
P7
P9
P11
P13
P30
B
P7 Sense
P30 Sense

Figure S6

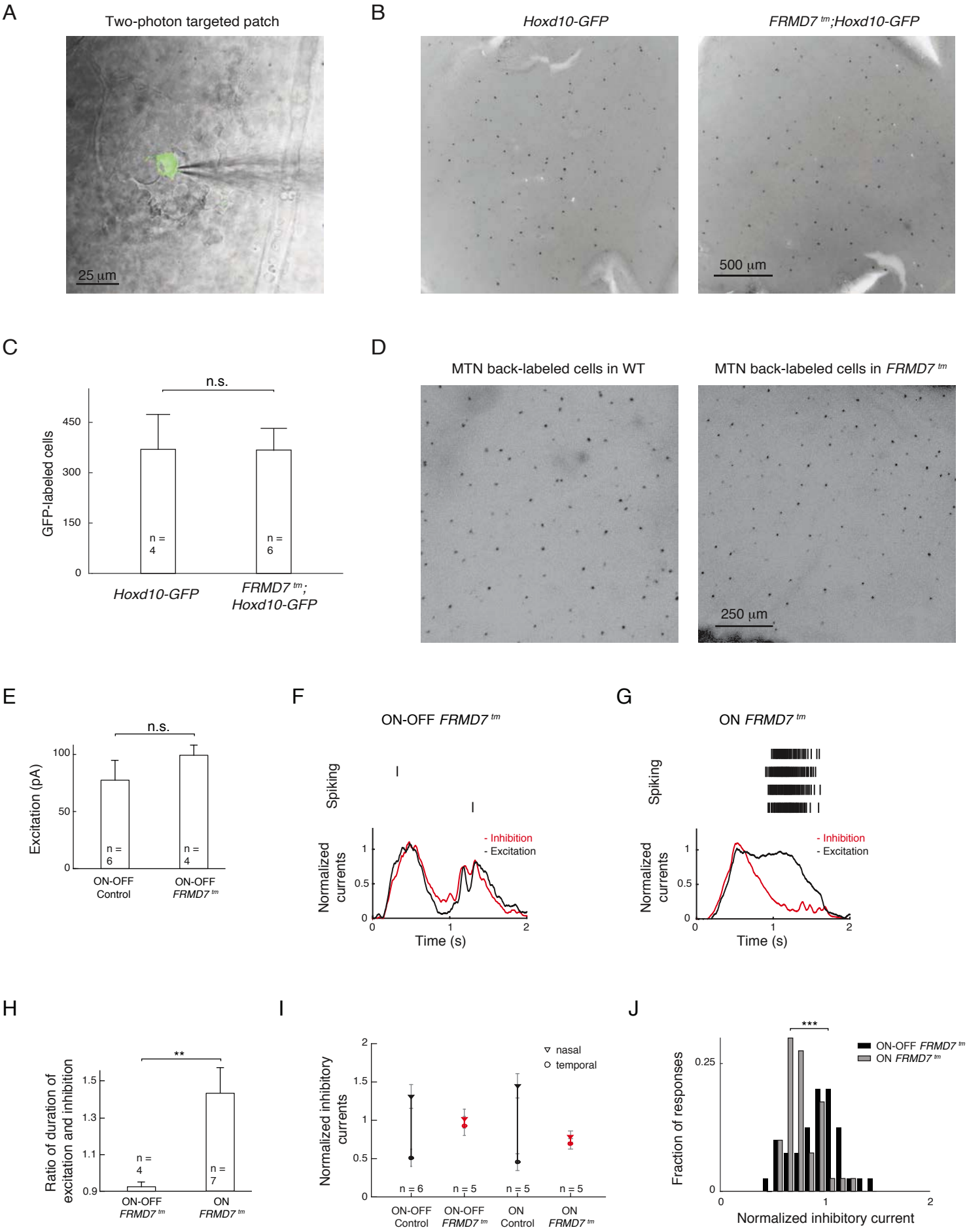
A
Two-photon targeted patch
25 μm
B
Hoxd10-GFP
FRMD7 tm;Hoxd10-GFP
500 μm
C
n.s.
GFP-labeled cells
450
300
150
0
n = 4
n = 6
Hoxd10-GFP
FRMD7 tm; Hoxd10-GFP
D
MTN back-labeled cells in WT
MTN back-labeled cells in FRMD7 tm
250 μm
E
n.s.
Excitation (pA)
100
50
0
n = 6
n = 4
ON-OFF Control
ON-OFF FRMD7 tm
F
ON-OFF FRMD7 tm
Spiking
Normalized currents
- Inhibition
- Excitation
1
0.5
0
0
1
2
Time (s)
G
ON FRMD7 tm
Spiking
Normalized currents
- Inhibition
- Excitation
1
0.5
0
0
1
2
Time (s)
H
**
Ratio of duration of excitation and inhibition
1.5
1.3
1.1
0.9
n = 4
n = 7
ON-OFF FRMD7 tm
ON FRMD7 tm
I
Normalized inhibitory currents
2
1.5
1
0.5
0
nasal
temporal
n = 6
n = 5
n = 5
n = 5
ON-OFF Control
ON-OFF FRMD7 tm
ON Control
ON FRMD7 tm
J
***
Fraction of responses
0.25
0
ON-OFF FRMD7 tm
ON FRMD7 tm
0
1
2
Normalized inhibitory current

Figure S7

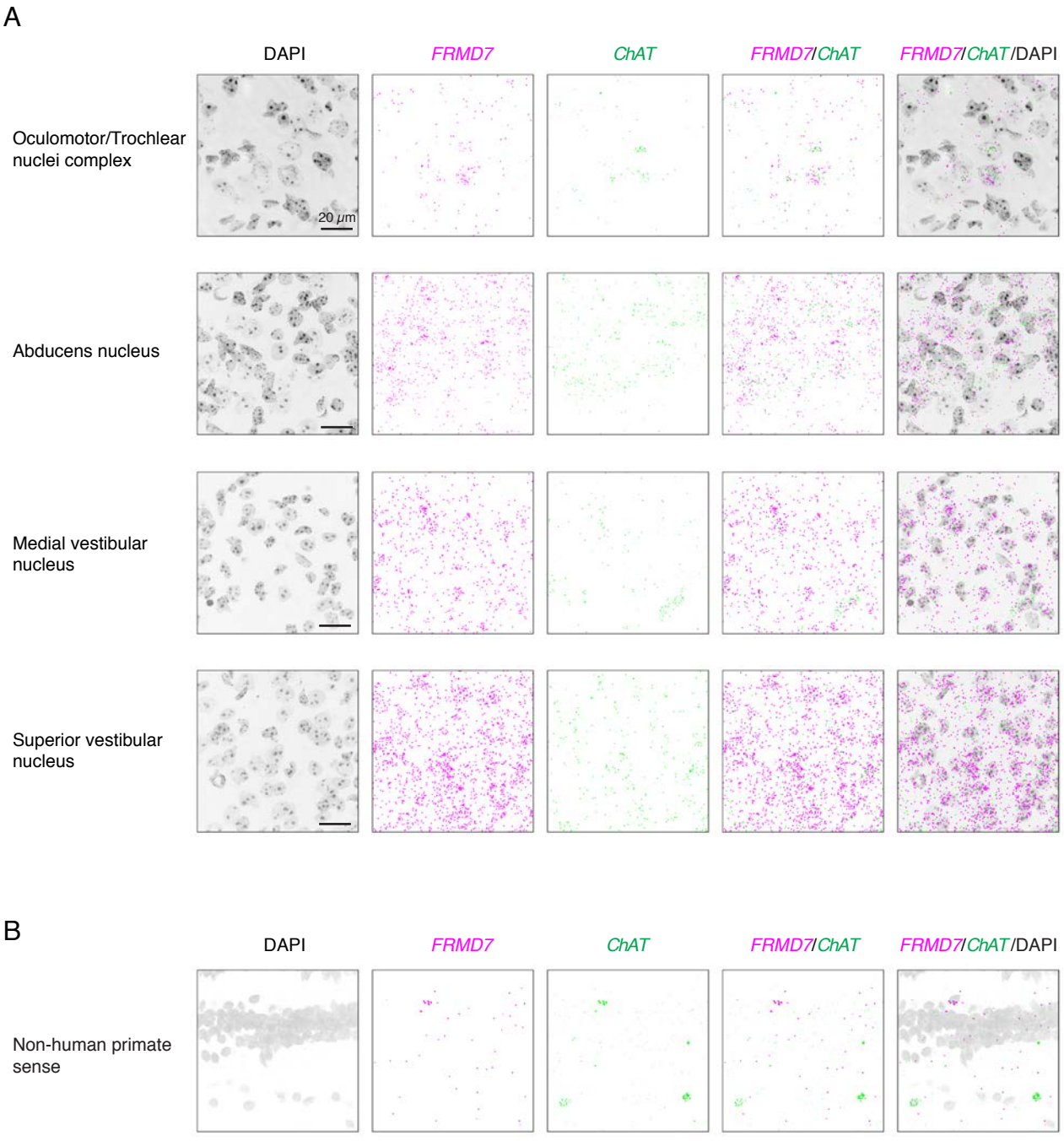
A
DAPI
FRMD7
ChAT
FRMD7/ChAT
FRMD7/ChAT/DAPI
Oculomotor/Trochlear nuclei complex
20 μm
Abducens nucleus
Medial vestibular nucleus
Superior vestibular nucleus
B
DAPI
FRMD7
ChAT
FRMD7/ChAT
FRMD7/ChAT/DAPI
Non-human primate sense

SUPPLEMENTAL FIGURE LEGENDS

Figure S1. Identification of *FRMD7* transcript variants in wild type and *FRMD7^{tm}* mice, related to Figures 1 and 3

(A) Schematic representation of predicted mRNAs in wild type (WT) and *FRMD7^{tm}* mice together with the primer locations (sequences corresponding to the names are shown in Experimental Procedures) and predicted RT-PCR products (P1-P7). Numbers (1-12) refer to the corresponding exon. The En2 fragment and iRES-LacZ are part of the cassette used to generate *FRMD7^{tm}* knock-in mice. (B) Agarose gel electrophoresis of the RT-PCR products of *FRMD7* mRNA in wild type (WT) and *FRMD7^{tm}* mice. Names of specific lanes correspond to predicted PCR products indicated in A. (C) Schematic representation of different *FRMD7* transcript variants cloned and sequenced from *FRMD7^{tm}* mice. Asterisks indicate frame-shift-generated stop codons. (D) RT-qPCR quantified expression levels of *FRMD7* transcript variants in *FRMD7^{tm}* mice. Individual transcripts were amplified using the oligonucleotide primers indicated in brackets. Expression level of the FRMD7-Mut-ex4-del transcript variant was determined by subtracting the level of FRMD7-WT (ex3F/ex4R primer pair amplified) transcript from the level of ex3F/ex5R primer pair amplified transcripts. (E) Comparison of the expression of FRMD7-WT transcript in wild type and *FRMD7^{tm}* mice using RT-qPCR. (F) LacZ is specifically expressed in starburst cells in the retina of *FRMD7^{tm}* mice. Confocal images of the GCL (top) and INL (bottom) of adult *FRMD7^{tm}* retina stained with antibodies for LacZ and ChAT. Black arrows indicate clustered LacZ signals.

Figure S2. Nystagmus and optokinetic reflex, related to Figure 1. (A) Eye movements produced by wild type (black) and *FRMD7^{tm}* (red) mice in response to motion in the superior direction on the retina. (B) Distribution of fixation points during fixation in a control human subject (left) and a subject with *FRMD7* mutation (right). (C) Quantification of data in B using the full-width-at-half-maximum values (FWHM) of fitted 2D Gaussian curves. (D) Power spectra (red traces, arbitrary units) of the horizontal (top) and vertical eye movements (bottom) of a human subject with *FRMD7* mutation during fixation (left) and during visual stimulation with gratings moving at 15 degrees/second (right). The panels demonstrating eye motion during motion stimulation also show the power spectrum of the visual stimulation (black traces). Note that the power spectra of stimulation and eye motion do not overlap when the human subject was stimulated with horizontal motion, but do overlap when stimulated with vertical motion.

Figure S3. Visual responses of retinal ganglion cells in wild type and *FRMD7^{tm}* mice, related to Figure 2. The figure shows data obtained with microelectrode arrays. Black is wild type, red is *FRMD7^{tm}*. (A) Distributions of the number of spikes in response to flashed stimuli in all recorded ganglion cells. (B) Distributions of peak responses to fast (left) and slow (right) motion stimulation in non-DS (DSI < 0.1) ganglion cells. (C) Upper panels, distribution of DSI in response

to fast (left) and slow (right) motion in all ganglion cells. Lower panels, same as shown in upper panels but only cells having a DSI of 0.5-1 are shown. (D) Velocity tuning of ON-OFF and ON cells. Number of spikes (normalized to the maximum) evoked by motion at different velocities in ON-OFF (left) and ON (right) cells. Error bars indicate SD.

Figure S4. Lack of horizontal direction selectivity in ON-OFF and ON cells in the retina of *FRMD7^{tm}* mice, related to Figure 2. The figure shows data obtained with microelectrode arrays. In A-C, the left two columns show ON-OFF DS cells and the right two columns ON DS cells (Experimental Procedures). The radius of each circle corresponds to DSI=1. (A) Polar plots showing the preferred directions (direction of an arrow) and direction selectivity index (DSI, length of an arrow) of individual DS cells (DSI > 0.5, each recorded DS cell is represented by an arrow) in wild type and *FRMD7^{tm}* retinas. The color code designates the different directions according to Figure 1A. (B) Contour plots showing the density of DS cells with different DSIs and preferred directions. Red indicates maximal density. (C) The proportion of horizontal (nasal and temporal) and vertical (superior and inferior) motion preferring DS cells in wild type and *FRMD7^{tm}* retinas. (D-F) Lack of horizontal direction selectivity in the retina of *FRMD7^{tm}* mice at P13/14. (D) Polar plots showing the preferred directions (direction of arrow) and direction selectivity index (DSI, length of arrow) of individual DS cells (DSI > 0.5, each recorded DS cell is represented by an arrow) in wild type and *FRMD7^{tm}* retinas. The color code designates the different directions according to Figure 1A. (E) Contour plots showing the density of DS cells with different DSIs and preferred directions. Red indicates maximal density. (F) The proportion of horizontal (nasal and temporal) and vertical (superior and inferior) motion preferring DS cells in wild type and *FRMD7^{tm}* retinas.

Figure S5. FRMD7 is specifically expressed in starburst cells in the mouse retina during development, related to Figure 3. (A) Confocal images of mouse retinal sections stained by double-label fluorescence *in situ* hybridization using antisense probes for mouse *FRMD7* mRNA and mouse *ChAT* mRNA as well as DAPI at different developmental stages. Large dots at E12.5 and E16.5 are non-specific signals. (B) Confocal images of mouse retinal section stained using sense probe for mouse *FRMD7* mRNA and antisense probe for mouse *ChAT* mRNA as well as DAPI at P7 and P30.

.

Figure S6. Characterization of genetically labeled DS cells in the retina of *FRMD7^{tm}* mice, related to Figures 4 and 5. (A) Overlay of infrared image (black-white) and two-photon microscope image (green) of the ganglion cell layer of *Hoxd10-GFP* mice during two-photon targeted patch-recording. GFP-labeled DS cell (green, center) is being recorded in cell-attached mode using a glass-pipette (dark shape on right side of green cell). (B) Epi-fluorescence microscope images of GFP-labeled cells (black) in fixed retinas after immunostaining in *Hoxd10*-GFP (left) and *FRMD7^{tm};Hoxd10-GFP* (right) mice. (C) Quantification of GFP-labeled cells counted in unstained, freshly dissected *Hoxd10*-GFP and

FRMD7^{tm};*Hoxd10-GFP* retinas. Data points represent mean ± SEM, n refers to the number of retinas. (D) Epi-fluorescence microscope images of MTN back-labeled cells (black) in wild type (left) and *FRMD7^{tm}* (right), unstained, dissected retinas. (E) Bar graph displaying amplitudes of excitatory input current to GFP-labeled ON-OFF cells in *Hoxd10*-GFP (Control) and *FRMD7^{tm}*;*Hoxd10-GFP* (*FRMD7^{tm}*) retinas. Data points represent mean ± SEM, n refers to the number of cells. (F, G) Spike raster plot (top, black, four repetitions) and normalized excitation (bottom, black) and inhibition (bottom, red) recorded in ON-OFF (F) and ON (G) example cells of *FRMD7^{tm}*;*Hoxd10-GFP* mice in response to motion. (H) Bar graph displaying the ratio of the duration of excitation and inhibition in ON-OFF cells and ON cells recorded in *FRMD7^{tm}*;*Hoxd10-GFP* mice. Data from the eight motion directions were averaged. Data points represent mean ± SEM, n refers to the number of cells. (I) Magnitudes of inhibitory currents evoked by stimulation with temporal (circles) or nasal (triangles) motion recorded in ON-OFF cells and (non-vertically tuned) ON cells in *Hoxd10*-GFP (Control, black) and *FRMD7^{tm}*;*Hoxd10-GFP* (*FRMD7^{tm}*, red) retinas. Values were normalized by the magnitude of inhibitory current evoked by a flashed-spot stimulus. Data points represent median values, temporal and nasal median values are connected with solid lines, ± SEM is shown by gray bars, n refers to the number of cells. (J) Histogram showing the distribution of inhibitory current magnitudes evoked by motion in eight directions recorded in ON-OFF cells (black, n=5) and (non-vertically tuned) ON cells (grey, n=5) in *FRMD7^{tm}*;*Hoxd10-GFP* retinas. Values were normalized by the magnitude of inhibitory current evoked by a flashed spot stimulus.

Figure S7. **FRMD7 is expressed in motor nuclei, which innervate extraocular muscles, and vestibular nuclei, related to Figures 6 and 8.** (A) Confocal images of oculomotor/trochlear nuclei complex (top), abducens nucleus (second row), medial vestibular nucleus (third row) and superior vestibular nucleus (bottom) of P11 wild type mouse brain sections stained by double-label fluorescence *in situ* hybridization using antisense probes for *FRMD7* mRNA and *ChAT* mRNA as well as DAPI. (B) Confocal images of non-human primate retinal section stained using sense probe for non-human primate *FRMD7* mRNA and antisense probe for non-human primate *ChAT* mRNA as well as DAPI.

Movie S1. Horizontal optokinetic reflex in head fixed wild type (left) and *FRMD7^{tm}* (right) mice, related to Figure 1. Stimulus is shown at the bottom.

EXTENDED EXPERIMENTAL PROCEDURES

Animals. Wild type mice (C57BL/6) were obtained from Charles River. *FRMD7^{tm}* mice refer to the homozygous female or hemizygous male *Frmd7$^{tm1a(KOMP)Wtsi}$* mice, which were obtained from the Knockout Mouse Project (KOMP)

Repository. A splicer acceptor-*IRES-lacZ* cassette is inserted into the intron between *FRMD7* exon 3 and exon 4, designed to result in the production of a truncated N-terminal part of the FRMD7 protein (68 amino acids) and LacZ. The integrity of the targeted genomic region in the *FRMD7*^{tm} mouse was confirmed by PCR by the International Mouse Phenotyping Consortium (IMPC). Genotyping of *FRMD7*^{tm} mice was carried out according to KOMP instructions. Both male and female *FRMD7*^{tm} mice were used in this study. The mRNA variants expressed from the mutant *FRMD7* locus in *FRMD7*^{tm} mice are described below in the section "Mouse FRMD7 mRNA analysis". *ChAT-Cre* mice (Ivanova et al., 2010) were obtained from Jackson Laboratory (strain: B6;129S6-*Chat*$^{tm1(cre)Lowl}$/J) and *Hoxd10-GFP* mice (Dhande et al., 2013) from Mutant Mouse Research and Resource Center (strain: STOCK Tg*(Hoxd10-EGFP)LT174Gsat/Mmucd*). Unless indicated otherwise, mice were between age P40 and P120. Mice were maintained in C57BL/6 background. A female cynomolgus monkey (Macaca fascicularis), was obtained from BioPRIM. Animals were housed in groups under maintained temperature (20-24°C), at least 40% humidity and a natural light cycle, and fed at least twice daily with a mixture of fruits and vegetables. Water and Kliba Nafag 3446 pellets (Kaiseraugst, Germany) were provided ad libitum. Euthanasia at age 19 was performed by intravenously applied 10 ml pentobarbital (Esconarkon, Streuli Pharma AG, Uznach, Switzerland). All animal procedures were performed in accordance with standard ethical guidelines (European Communities Guidelines on the Care and Use of Laboratory Animals, 86/609/EEC) and were approved by the Veterinary Department of the Canton of Basel-Stadt, Switzerland.

Human subjects. Eye movement was recorded from three male human subjects with congenital nystagmus (ages 19, 22 and 41) resulted from a hemizygous mutation in the FRMD7 gene as well as from four control subjects (ages 30, 30, 33, and 36). Human subjects with congenital nystagmus had a complete ophthalmologic examination, including slit-lamp examination, fundus examination and measurement of visual acuity. The mutations were c.685C>T (p.R229C) in exon 8 in the 19 and 22 year old subjects (from the same family) and c.673T>G (p.W225G) in exon 8 in the 41 year old subject. This prospective research was conducted in accordance with Good Clinical Practices. The research procedures followed the tenets of the Declaration of Helsinki, and all tests and examinations were performed after obtaining informed consent from all subjects. The study protocol was approved by the relevant Institutional Review Boards.

Eye movement detection. Eye tracking was performed using an ETL-200 eye tracking system (Iscan Inc., Woburn, Maine, USA). To visualize the pupil, eyes were illuminated with IR light and recorded with IR cameras, at 240 Hz in humans, and at 120 Hz in mice. The optokinetic reflex was quantified by counting the number of eye tracking movements (ETMs) as described previously (Cahill and Nathans, 2008). Briefly, the position of the pupil was plotted as a function of time, the derivative of this signal was calculated and a threshold was set. Events above threshold were counted as ETMs.

The threshold was adjusted in wild type mice and in control human subjects so that all visually assessed ETMs were detected. This threshold was then applied to data from *FRMD7*^{tm} mice and human subjects with *FRMD7* mutation.

Visual stimulation, controlled by software written in Python (python.org), or PsychoPy (psychopy.org), was presented on a computer monitor. For humans, the monitor was placed 65 cm from the eye, which corresponded to 44° of visual angle horizontally and 28° vertically. The head was kept in place with a chin rest. For eye fixation, a spot of 0.25° diameter was presented for 15 s in the center of the monitor. For motion stimulation, black and white gratings (0.5 duty cycle) with 6° wide bars were moved at 15°/s. One degree corresponds to 300 μm retinal distance in humans (Oyster, 2006). For mice, visual stimulation was executed as described previously (Yonehara et al., 2009), except that here two monitors were placed in a 'V' position in front of the mouse for binocular stimulation. The head of the mouse was fixed with a head holder, and the body was restrained in a foam jacket. For motion stimulation black and white gratings (0.5 duty cycle) with 20°-wide bars were moved at 10°/s. One degree corresponds to 31 μm retinal distance in mice (Remtulla and Hallett, 1985).

AAV production. To obtain the production plasmid for serotype-7 AAV-EF1a-DIO-TVA66T-WPRE-hGHpA, we linearized pAAV-EF1a-double floxed-hChR2(H134R)-EYFP-WPRE-hGHpA (kindly provided by K. Deisseroth, Stanford University) using NheI/AscI sites. A TVA66T insert with NheI/AscI overhand sites was synthesized (GenScript) based on the CAG-Flex-TC66T sequence, which was obtained from Addgene (plasmid # 48331) and cut using NheI/AscI. pAAV-hSyn1(S)-FLEX-tdTomato-T2A-SypEGFP-WPRE was obtained from Addgene (plasmid # 51509). AAV was made according to standard protocols. Genome copy (GC) number titration was performed using real-time PCR (Applied Biosystems, TaqMan reagents).

Rabies virus production. G-coated SADΔG-GFP rabies virus (Wickersham et al., 2007a)(provided by K.K. Conzelmann, Munich) was amplified by infecting B7GG cells. EnvA-coated SADΔG-GFP rabies virus was obtained by infecting BHK-EnvARGCD cells with the G-coated viruses (Wickersham et al., 2007b). Viruses were concentrated by ultracentrifugation as described before (Ghanem et al., 2012). Titration using plaque-forming units (pfu) was performed by infecting BHK cells and HEK293T-TVA800 cells with G-coated virus and EnvA-coated virus, respectively.

Virus injections. Mice were anesthetized with an intraperitoneal injection of ketamine (108 mg/kg) and xylazine (14.4 mg/kg). To label starburst cells with GFP, serotype-7 AAV-EF1a-DIO-TVA66T-WPRE-hGHpA in PBS (1.8×10^{15} GC/ml) was loaded into pulled-glass pipettes (tip inner diameter 20-30 μm) and 2 μl was injected intravitreously into the

eye of *ChAT-Cre* and *FRMD7^{tm}*;*ChAT-Cre* mice using a pneumatic microinjector (Narishige, IM-11-2). Two weeks later, EnvA-coated SADΔG-GFP rabies virus (10^{10} pfu/ml) was loaded into pulled-glass pipettes and 2 µl was injected intravitreously into the eye. One week later the retinas were isolated and fixed with 4% paraformaldehyde. To label starburst cells with synaptophysin-GFP, serotype-8 AAV-hSyn1(S)-FLEX-tdTomato-T2A-SypEGFP-WPRE-hGHpA (3.72×10^{11} GC/ml) was loaded into a Hamilton syringe and 2 µl was injected intravitreously into the eye of *ChAT-Cre* and *FRMD7^{tm}*;*ChAT-Cre* mice. Three weeks later the retinas were isolated and fixed with 4% paraformaldehyde.

Fluorescent *in situ* hybridization. Double-label fluorescent *in situ* hybridization on retinal sections from mice and non-human primate, and brain sections from mice was carried out using the RNAscope Multiplex Fluorescent Assay (Advanced Cell Diagnostics) according to the manufacturer's instructions. Briefly, dissected retinas were fixed with 4% paraformaldehyde, cryoprotected with 30% sucrose in PBS, embedded in OCT compound, frozen on dry ice, and cryosectioned at 20 µm. To prepare embryonic retinal sections, embryos were fixed overnight in 4% paraformaldehyde in PBS and washed with PBS for at least 1 day at 4°C, cryoprotected with 30% sucrose in PBS, embedded in OCT compound, frozen on dry ice, and cryosectioned at 20 µm. To prepare brain sections, animals were transcardially perfused with 4% paraformaldehyde and the brains were post-fixed in 4% paraformaldehyde overnight at 4°C, cryoprotected with 30% sucrose in PBS, embedded in OCT compound, frozen on dry ice, and cryosectioned at 30 µm. Mouse retinal or brain sections were hybridized with antisense and sense probes for mouse *FRMD7* mRNA (Genbank: NM_001190332.1) and antisense probe for mouse *ChAT* mRNA (Genbank: NM_009891.2), and signals were amplified. Non-human primate retinal sections were hybridized with antisense and sense probes for macaca fasicularis *FRMD7* mRNA (Genbank: XM_005594586.1) and antisense probe for macaca fasicularis *ChAT* mRNA (Genbank: XM_005565136.1), and signals were amplified. Slides were stained with DAPI and mounted with Prolong Gold (Life Technologies). Positive staining was identified as punctate dots present within the cells.

Retrograde and anterograde tracer injections. To label ON DS cells projecting to the MTN, adult mice were anesthetized with an intraperitoneal injection of ketamine/xylazine and head-fixed with a stereotaxic instrument (Narishige, SR-5M). Cholera toxin subunit B Alexa Fluor 488 conjugate (Invitrogen, C34775) at 1 mg/µl in PBS was loaded into pulled-glass pipettes (tip inner diameter 20-30 µm), and 100 µl was injected into the MTN using a pneumatic microinjector (Narishige, IM-11-2).

To label retinal ganglion axons innervating retino-recipient nuclei, mice were anesthetized with an intraperitoneal injection of ketamine/xylazine. Cholera toxin subunit B Alexa Fluor 594 conjugate (Invitrogen, C34777) or 647

conjugate (C34778) at 1 mg/µl in PBS was loaded into pulled-glass pipettes (tip inner diameter 20-30 µm) and 2 µl was injected intravitreously into the eye. One week later brains were isolated and used for immunohistochemistry.

Preparation of retina for electrophysiology. Light-adapted mice were used for recordings. Retinas were isolated under dim red light (FGL610, Thorlabs) in Ringer's medium (in mM: 110 NaCl, 2.5 KCl, 1 $CaCl_2$, 1.6 $MgCl_2$, 10 d-glucose, 22 $NaHCO_3$) bubbled with 5% CO_2, 95% O_2. The dorsal side of the retina was marked with a small incision, which was later used to align the visual stimulation to the retinal axes. For microelectrode array recordings, a retinal patch was placed ganglion-cell-side-down on the microelectrode array. To secure the retina on the microelectrode array, a permeable membrane (polyester, 10 µm thickness, 0.4 µm pore size) was lightly pressed against the tissue. For patch-clamp recordings, the retina was mounted ganglion-cell-layer-up on a filter paper (Millipore) with a 2×2 mm aperture to allow for visual stimulation of the photoreceptors. During microelectrode array and patch-clamp recordings, the retina was kept at 35°C and was continuously superfused with Ringer's medium bubbled with 5% CO_2, 95% O_2.

Microelectrode array recordings. Recordings and light stimulation were performed as described before (Fiscella et al., 2012). In most experiments, CMOS-based microelectrode arrays with 11,011 platinum electrodes with diameters of 7 µm and electrode center-to-center distances of 18 µm over an area of 2×1.75 mm^2 were used (Fiscella et al., 2012; Frey et al., 2009, 2010). In some experiments CMOS-based microelectrode arrays with 26,400 platinum electrodes over an area of 3.85×2.1 mm^2 and 1,024 readout channels and a center-to-center electrode distance of 17.5 µm were used (Ballini et al., 2014; Müller et al., 2015) .

Visual stimuli. Flashed stimulus: this stimulus was used to determine if a cell was ON-OFF (responding to both light increments and decrements) or ON (responding to light increments only). A positive-contrast square stimulus (0.2×0.2 mm^2) was turned on for one second and turned off for one second in 5 repetitions. The stimulus moved sequentially in discrete non-overlapping steps over an area of ~1 mm^2 with a background irradiance of 0.2 µW/cm^2 and a square stimulus irradiance of 47 µW/cm^2. Motion stimulus: this stimulus was used to test direction selectivity. A 1 mm wide and 0.5 mm long (perpendicular to stimulus motion) white bar (background irradiance 0.2 µW/cm^2 and stimulus irradiance 47 µW/cm^2) moved across the retina at a velocity of 0.15 or 0.8 mm/s, along eight equidistant angular directions radially spaced at 45°. The large bar width (1 mm) was chosen to separate ON and OFF responses. Each motion stimulus was repeated five times.

Spike sorting and data analysis. For spike sorting we used a fully automatic two-stage procedure that first identified spike templates for each neuron (Marre et al., 2012; Prentice et al., 2011) and then classified each spike using template matching (Franke et al., 2015). Spike data obtained from stimulus repetitions were averaged. The direction selectivity index (DSI) and preferred direction of a neuron were defined as described previously (Taylor and Vaney 2002). Briefly, eight vectors were formed, each associated with motion along a direction. The length of each vector was the mean number of spikes across stimulus repetitions along the relevant direction and the angle of the vector was the angle corresponding to the motion direction (0°, 45°, 90°, 135°, 180°, 225°, 270°, 315°). The DSI and preferred direction of the neuron were defined as the length and angle of the sum of the eight vectors divided by the sum of the lengths of the eight vectors (normalized vector sum), respectively. The horizontal and vertical DSIs were defined as the length of the horizontal and vertical components of the normalized vector sum. In the analysis of microelectrode electrode array data, we defined a neuron as direction selective if its DSI was higher than 0.5.

Slow- and fast-motion preferring DS cells were segregated using a velocity index (VI).

$$VI = (rF - rS)/(rS + rF)$$

rF is the maximum response of a cell across the eight stimulus directions using a motion velocity of 0.8 mm/s, and rS is the maximum response of the same cell across the eight stimulus directions using a motion velocity of 0.15 mm/s. VI ranges from −1 to 1. Cells with $VI > -0.5$ were categorized as fast DS cells and with $VI \leq -0.5$ as slow DS cells.

ON-OFF and ON DS cells were segregated using an ON-OFF index (OOI).

$$OOI = (rON - rOFF)/(rON + rOFF)$$

rON is the maximum response of a cell to a positive contrast, flashed stimulus stepped across its receptive field, and rOFF is the maximum response of a cell to a negative contrast, flashed stimulus stepped across its receptive field. The OOI ranges from −1 to 1. Cells with $|OOI| < 0.8$ were categorized as ON-OFF cells and cells with $OOI > 0.8$ as ON cells.

Two-photon targeted patch clamp recording. *Hoxd10-GFP* and *FRMD7^{tm}*;*Hoxd10-GFP* mice were used for targeted recordings. Cells back-labeled from the MTN with cholera toxin subunit B Alexa Fluor 488 conjugate were targeted to record from vertically tuned ON DS cells in wild type and *FRMD7^{tm}* mice. The two-photon microscope system for targeted patch clamp recordings from GFP- or Alexa488-labeled cells, including the light pathways for visual stimulation of the retina, has been described before (Farrow et al., 2013). GFP- or Alexa488-labeled cells were targeted using a two-photon microscope equipped with a Mai Tai HP two-photon laser (Spectra Physics), set to 920 nm, which was integrated into the electrophysiological setup. The two-photon fluorescence image was overlaid on an IR image acquired with a

CCD camera (SPOT Visitron Systems). The infrared light was produced with a digital light projector (V300X, NEC) and a 750 ± 25 nm filter. Spike recordings and whole-cell recordings were performed with borosilicate glass electrodes (BF100-50-10, Sutter Instruments), pulled to 5-7 MΩ, using an Axon Multiclamp 700B amplifier. Signals were digitized at 10 kHz and acquired using software written in LabVIEW (National Instruments). Spike recordings were made in loose cell-attached mode and electrodes were filled with Ringer's solution. Whole-cell recordings were made in voltage-clamp mode and electrodes were filled with (in mM) 112.5 $CsCH_3SO_3$, 1 $MgSO_4$, 7.8×10^{-3} $CaCl_2$, 0.5 BAPTA, 10 HEPES, 4 ATP-Na_2, 0.5 GTP-Na_3, 5 lidocaine N-ethylbromide (Qx314-Br) and 7.75 neurobiotin chloride; pH adjusted to 7.2. Inhibitory and excitatory currents ('inhibition' and 'excitation') were separated by voltage clamping the cell to the equilibrium potential of unselective cation channels (0 mV) or the equilibrium potential of chloride (−60 mV), respectively (Roska and Werblin, 2001). The light for retinal stimulation was generated by a digital light projector (V300X, NEC) at a refresh rate of 75 Hz, and focused on the retinal photoreceptor layer after passing a neutral density filter (ND40). After targeting, the recorded cell was kept at a constant grey background level with a light intensity of 60 $\mu W/cm^2$ on which the positive or negative contrast stimulus was displayed. The moving stimulus consisted of a 300 µm-diameter light spot with positive 50% contrast (122 $\mu W/cm^2$), which moved across the retina in eight directions at 300 µm/s. The flashed stimulus consisted of a 300 µm-diameter light spot with positive or negative 50% contrast centered to the soma of the cell. All stimuli were repeated five times. The visual stimulation was controlled via custom-made software written in Python (Python Software Foundation).

Data were analyzed offline using MATLAB (Mathworks). Spikes were detected by thresholding. Spike data and inhibitory currents were averaged across stimulus repetitions. Responses were quantified by counting the spike events for the cell-attached data and measuring the amplitude of the inhibitory current for the whole-cell data for each motion direction. From these responses the DSI and the horizontal DSI were computed for both spike tuning and inhibitory tuning, as described in the microelectrode array section. Polar plots of the spike tuning and quantification of spiking DSI were only made for cells responding with at least 15 spikes in four stimulation trials. Spike rates were obtained by convolving the spike train with a Gaussian window (sigma = 35 ms). Inhibitory current traces were smoothed using the MATLAB smooth function with a span of 0.3 s for plotting the example cells (Figures 4-5) or a span of 0.01 s for plotting the time course of inhibition and excitation (Figures S6F-S6G). The duration of excitatory and inhibitory currents was defined by the time, during which the current was higher than 75% of its maximal value. For normalization of motion-evoked magnitudes of inhibitory currents, values were divided by the magnitude of the inhibitory current evoked by the flashed spot stimulus for each cell.

Mouse *FRMD7* mRNA analysis. Total RNA was extracted from wild type and *FRMD7*^{tm} retinas using Trizol reagent (Invitrogen). To form cDNA, RNA was reverse transcribed using random hexamers and the Superscript III thermostable RT system (Invitrogen) according to the manufacturer's instructions. *FRMD7* splice variants were determined from wild type and *FRMD7*^{tm} cDNA by PCR amplification using the following primers: ex2F (5'-cgctcttcaacctgagctg), ex3R (5'-cttgcttcgttatgggcttc), ex3F (5'- tggaacttctgaagcccataa), ex4R (5'-agttcttcccgaagatgtcc), ex5R (5'-atgtgcgacaccattaaagc), En2R (5'-aactcagccttgagcctctg), lacZR1 (5'-caccacgctcatcgataattt), lacZF1 (5'-ttcaacatcagccgctacag), and lacZR2 (5'-tttcaggttcaggggaggtgtg) (Figure S1A). PCR products were identified on agarose gel (Figure S1B), extracted, cloned using the TOPO Cloning Kit (Invitrogen) and sequenced, and the sequences were analyzed (Figures S1C-S1E). In wild type mice we identified a single transcript variant across exon 2 to exon 5 (FRMD7-WT, see below). In *FRMD7*^{tm} mice we found three major transcript variants (FRMD7-Mut, FRMD7-Mut-ex4-del and FRMD7-WT). FRMD7-Mut-ex4-del had two minor variants (FRMD7-Mut-ex4-del-v1 and FRMD7-Mut-ex4-del-v2). The FRMD7-Mut transcript contains the first three exons of *FRMD7* mRNA and the non-genomic *En2-IRES-LacZ* cassette. In FRMD7-Mut-ex4-del-transcripts exon 4 is deleted. Due to inserted, in-frame stop codons, both FRMD7-Mut and FRMD7-Mut-ex4-del transcripts are predicted to produce a truncated protein consisting of exons 1 to 3 in which the FERM-N domain of *FRMD7* is disrupted and FERM-M and FERM-C domains omitted. The presence of (low levels of) wild type transcript is likely due to alternative splicing that skips the inserted *LacZ* cassette. The 5-prime region of the *FRMD7* transcript variants (Figure S1C) are shown below, the first in-frame stop codon is shown underlined and bold, the primer pair used to amplify the transcript fragment is shown in brackets.

FRMD7-Mut (ex3F/lacZR1):

tggaacttctgaagcccataacgaagcaagtcaaaaatcccaggtcccgaaaaccaaagaagaagaaccctaacaaagaggacaagcggcctcgcacagccttcactgctga
gcagctccagaggctcaaggctgagtttcagaccaacaggtacctgacagagcagcggcgccagagtctggcacaggagctcggtacccggaagatctggactctagagaa
ttccgcccctctccctccccccccccctaacgttactggccgaagccgcttggaataaggccggtgtgcgtttgtctatatgttatttttccaccatattgccgtcttttggcaatg**tga**gg
gcccggaaacctggccctgtcttcttgacgagcattcctaggggtctttcccctctcgccaaaggaatgcaaggtctgttgaatgtcgtgaaggaagcagttcctctggaagcttctt
gaagacaaacaacgtctgtagcgacccttttgcaggcagcggaacccccccacctggcgacaggtgcctctgcggccaaaagccacgtgtataagatacacctgcaaaggcgg
cacaaccccagtgccacgttgtgagttggatagttgtggaaagagtcaaatggctctcctcaagcgtattcaacaaggggctgaaggatgcccagaaggtaccccattgtatggg
atctgatctggggcctcggtgcacatgctttacatgtgtttagtcgaggttaaaaaacgtctaggccccccgaaccacggggacgtggttttcctttgaaaaacacgatgataagctt
gccacaaccatggaagatcccgtcgttttacaacgtcgtgactgggaaaaccctggcgttacccaacttaatcgccttgcagcacatccccctttcgccagctggcgtaatagcga
agaggcccgcaccgatcgcccttcccaacagttgcgcagcctgaatggcgaatggcgctttgcctggtttccggcaccagaagcggtgccggaaagctggctggagtgcgat
cttcctgaggccgatactgtcgtcgtcccctcaaactggcagatgcacggttacgatgcgcccatctacaccaacgtgacctatcccattacggtcaatccgccgtttgttcccacg
gagaatccgacgggttgttactcgctcacatttaatgttgatgaaagctggctacaggaaggccagacgcgaattatttttgatggcgttaactcggcgtttcatctgtggtgcaacg

ggcgctgggtcggttacggccaggacagtcgtttgccgtctgaatttgacctgagcgcatttttacgcgccggagaaaaccgcctcgcggtgatggtgctgcgctggagtgacg
gcagttatctggaagatcaggatatgtggcggatgagcggcattttccgtgacgtctcgttgctgcataaaccgactacacaaatcagcgatttccatgttgccactcgctttaatgat
gatttcagccgcgctgtactggaggctgaagttcagatgtgcggcgagttgcgtgactacctacgggtaacagtttctttatggcagggtgaaacgcaggtcgccagcggcacc
gcgcctttcggcggtgaaattatcgatgagcgtggtg

FRMD7-Mut-ex4-del-v1(ex3F/ex5R):

tggaacttctgaagcccataacgaagcaagtcaaaaaggtatctttttactcttcaaataaagaaggatttggctctgggaaggcttccatgcag**tga**caactgcacagctttaatgg
tgtcgcacat

FRMD7-Mut-ex4-del-v2 (ex3F/ex5R):

tggaacttctgaagcccataacgaagcaagtcaaaaatccaggtatctttttactcttcaaa**taa**agaaggatttggctctgggaaggcttccatgcagtgacaactgcacagcttta
atggtgtcgcacat

FRMD7-WT (ex3F/ex5R):

tggaacttctgaagcccataacgaagcaagtcaaaaatcctaaggaggttgttttcaaatttatggtgaaatttttcccagtggaccccggacatcttcgggaagaactcacaaggt
atctttttactcttcaaataaagaaggatttggctctgggaaggcttccatgcagtgacaactgcacagctttaatggtgtcgcacat

In RT-qPCR analysis the level of the three major transcript variants were determined relative to 18S rRNA (Figures S1D-S1E). The phenotype observed in *FRMD7*^{tm} mice likely results from the significant decrease in the level of the FRMD7 protein. If, however, the truncated proteins made from the mutant transcripts are not degraded, it is possible that they act as dominant negative regulators of FRMD7 function.

Immunohistochemistry. Mouse retinas were fixed for 30 min in 4% (wt/vol) paraformaldehyde in PBS (in mM: 137 NaCl, 2.7 KCl, 4.3 Na_2HPO_4, 1.47 KH_2PO_4; pH 7.4) and washed with PBS for at least 1 day at 4°C. Non-human primate retinas were fixed for one or two days in 4% paraformaldehyde in PBS and washed with PBS for at least 1 day at 4°C. To stain the mouse brains, animals were transcardially perfused with 4% paraformaldehyde. The brains were post-fixed in 4% paraformaldehyde overnight at 4°C and sectioned at 150 µm using a vibratome (Leica, VT1000S). To aid penetration of the antibodies, retinas were frozen and thawed three times after cryoprotection with 30% (wt/vol) sucrose in PBS. For staining with anti-β galactosidase, antigen retrieval was carried out by incubating retinas in Tris-EDTA buffer (10 mM Tris, 1 mM EDTA, 0.05% Tween20, pH 8.0) for 30 min at 80°C. All other procedures were carried out at room temperature, except for the secondary antibody reaction. After washing in PBS, retinas were blocked for 1 h in 10%

(vol/vol) normal donkey serum (NDS; Chemicon), 1% (wt/vol) bovine serum albumin (BSA), and 0.5% (vol/vol) TritonX-100 in PBS. Primary antibodies were incubated for 6-7 days in 3% (vol/vol) NDS, 1% (wt/vol) BSA, 0.02% (wt/vol) sodium azide, and 0.5% (vol/vol) TritonX-100 in PBS. Secondary antibodies were incubated for one day at 4°C in 3% (vol/vol) NDS, 1% (wt/vol) BSA, and 0.5% (vol/vol) TritonX-100 in PBS together with streptavidin-Alexa Fluor 633 (Invitrogen, 1:200) and DAPI (4',6-diamidine-2-phenylindole dihydrochloride, Roche Diagnostics, 10 µg/ml) in some experiments. DAPI binds to DNA and, therefore, labels nuclei. After a final wash in PBS, retinas were embedded in Prolong Gold antifade (Life Technologies).

The following sets of primary and secondary antibody combinations were used for staining retinas:
(i) Primary: rabbit anti-FRMD7 (1:100). This affinity-purified polyclonal antibody was raised against the 16 amino acid C-terminal peptides of FRMD7 (Ac – SFATPGAEDRTLLKPC – NH2; Eurogentech). Secondary: donkey anti-rabbit IgG conjugated with Alexa Fluor 488 or 568 (1:200, Invitrogen). (ii) Primary: goat anti-ChAT (1:200, AB144P, Chemicon). Secondary: donkey anti-goat IgG conjugated with Alexa Fluor 488 or 568 (1:200, Invitrogen). (iii) Primary: rabbit anti-GFP (1:200, A11122, Invitrogen). Secondary: donkey anti-rabbit IgG conjugated with Alexa Fluor 488 (1:200, Invitrogen). (iv) Primary: rat anti-GFP (1:500, 04404-84, Nacalai). Secondary: donkey anti-rat IgG conjugated with Alexa Fluor 488 (1:200, Invitrogen). (v) Primary: chicken anti-β galactosidase (1:200, AB9361, abcam). Secondary: donkey anti-chicken IgY conjugated with Alexa Fluor 488 (1:200, Jackson ImmunoResearch).

Confocal analysis. Fluorescent *in situ* hybridization and immunohistochemistry signals in the retinas and brain sections were analyzed using a Zeiss LSM 700 confocal microscope. *In situ* hybridization signals were assessed from 1024×1024 pixel z-stack images at 0.35 µm z steps taken with a 63× oil immersion lens, numerical aperture (NA) 1.3. Immunohistrochemistry signals were assessed from 1024×1024 pixel z-stack images at 0.35 µm z steps taken with a 63× oil immersion lens, NA 1.3 or a 40× oil immersion lens, NA 1.0. Images were processed using Imaris (Bitplane), Fiji, or Mathematica (Wolfram). For quantification of fluorescent *in situ* hybridization, at each developmental time point (E12.5, E16.5, P1, P3, P5, P7, P9, P11, P13, and P30) we counted the number of punctuated dots for *ChAT* and *FRMD7* mRNAs present within the cell for five cells semi-automatically using the Imaris Spot function. To quantify the number of starburst cells in wild-type and *FRMD7*^{tm} retina, the ChAT-positive cells were counted manually from confocal images of anti-ChAT-stained retinas in Fiji. To quantify GFP-labeled starburst cell processes, we first drew a convex polygon by connecting the outer tips of the processes, and defined the area of the polygon as the dendritic field size in Fiji. For the dendritic asymmetry index, we determined the ratio between the widest and narrowest diameters of the polygon and expressed this as a percentage. The number of primary processes was counted in 3D-reconstructed confocal images in

Imaris. To quantify the co-stratification of neurobiotin-filled DS cell dendrites and anti-ChAT-labeled starburst cell processes in retinas of *Hoxd10-GFP* and *FRMD7^{tm}*;*Hoxd10-GFP* mice, we first determined the fluorescence intensity profile for neurobiotin and ChAT signals along the depth of the retina on the side view of the confocal z-stack in Fiji. Next, Full Width at Half Maximum for neurobiotin and ChAT signals were determined and their overlap at each of the proximal and distal strata within the inner plexiform layer was determined. To quantify GFP-labeled cells in the retinas of *Hoxd10-GFP* and *FRMD7^{tm}*;*Hoxd10-GFP* mice, the GFP-expressing cells were counted manually from epi-fluorescence stereomicroscopic (Olympus SZX16) images of non-stained, freshly dissected retinas.

Statistical Analysis. We used the following statistical tests. Mann-Whitney-Wilcoxon test: Figures 1C-1E, 1H-1J, 3C, 3E, 3H, 4E-4F, 5B, 5D, S1E, S2C, S6C, S6E, and S6H. Chi-square or Fisher exact test (if 'n' in a category ≤ 5): Figures 2C, S4C, and S4F. Hodges-Ajne test: Figure 7C. Kolmogorov-Smirnov test: Figures 2F, S3C and S6J. Statistical significance is noted by * for $p < 0.05$, ** for $p < 0.01$, and *** for $p < 0.001$. Not significant is denoted as n.s. for $p \geq 0.05$.

SUPPLEMENTAL REFERENCES

Ballini, M., Muller, J., Livi, P., Yihui Chen, Frey, U., Stettler, A., Shadmani, A., Viswam, V., Lloyd Jones, I., Jackel, D., et al. (2014). A 1024-Channel CMOS Microelectrode Array With 26,400 Electrodes for Recording and Stimulation of Electrogenic Cells In Vitro. IEEE J. Solid-State Circuits *49*, 2705–2719.

Cahill, H., and Nathans, J. (2008). The optokinetic reflex as a tool for quantitative analyses of nervous system function in mice: application to genetic and drug-induced variation. PloS One *3*, e2055.

Farrow, K., Teixeira, M., Szikra, T., Viney, T.J., Balint, K., Yonehara, K., and Roska, B. (2013). Ambient illumination toggles a neuronal circuit switch in the retina and visual perception at cone threshold. Neuron *78*, 325–338.

Franke, F., Quian Quiroga, R., Hierlemann, A., and Obermayer, K. (2015). Bayes optimal template matching for spike sorting - combining fisher discriminant analysis with optimal filtering. J. Comput. Neurosci.

Fiscella, M., Farrow, K., Jones, I.L., Jäckel, D., Müller, J., Frey, U., Bakkum, D.J., Hantz, P., Roska, B., and Hierlemann, A. (2012). Recording from defined populations of retinal ganglion cells using a high-density CMOS-integrated microelectrode array with real-time switchable electrode selection. J. Neurosci. Methods *211*, 103–113.

Frey, U., Egert, U., Heer, F., Hafizovic, S., and Hierlemann, A. (2009). Microelectronic system for high-resolution mapping of extracellular electric fields applied to brain slices. Biosens. Bioelectron. *24*, 2191–2198.

Frey, U., Sedivy, J., Heer, F., Pedron, R., Ballini, M., Mueller, J., Bakkum, D., Hafizovic, S., Faraci, F.D., Greve, F., et al. (2010). Switch-Matrix-Based High-Density Microelectrode Array in CMOS Technology. IEEE J. Solid-State Circuits *45*, 467–482.

Ghanem, A., Kern, A., and Conzelmann, K.-K. (2012). Significantly improved rescue of rabies virus from cDNA plasmids. Eur. J. Cell Biol. *91*, 10–16.

Marre, O., Amodei, D., Deshmukh, N., Sadeghi, K., Soo, F., Holy, T.E., and Berry, M.J. (2012). Mapping a complete neural population in the retina. J. Neurosci. Off. J. Soc. Neurosci. *32*, 14859–14873.

Müller, J., Ballini, M., Livi, P., Chen, Y., Radivojevic, M., Shadmani, A., Viswam, V., Jones, I.L., Fiscella, M., Diggelmann, R., et al. (2015). High-resolution CMOS MEA platform to study neurons at subcellular, cellular, and network levels. Lab Chip *15*, 2767–2780.

Oyster, C.W. (2006). The human eye: structure and function (Sunderland, Mass.; Basingstoke: Sinauer Associates ; Macmillan [distributor]).

Prentice, J.S., Homann, J., Simmons, K.D., Tkačik, G., Balasubramanian, V., and Nelson, P.C. (2011). Fast, scalable, Bayesian spike identification for multi-electrode arrays. PloS One *6*, e19884.

Remtulla, S., and Hallett, P.E. (1985). A schematic eye for the mouse, and comparisons with the rat. Vision Res. *25*, 21–31.

Roska, B., and Werblin, F. (2001). Vertical interactions across ten parallel, stacked representations in the mammalian retina. Nature *410*, 583–587.

Taylor, W.R., and Vaney, D.I. (2002). Diverse synaptic mechanisms generate direction selectivity in the rabbit retina. J. Neurosci. Off. J. Soc. Neurosci. *22*, 7712–7720.

Wickersham, I.R., Finke, S., Conzelmann, K.-K., and Callaway, E.M. (2007a). Retrograde neuronal tracing with a deletion-mutant rabies virus. Nat. Methods *4*, 47–49.

Wickersham, I.R., Lyon, D.C., Barnard, R.J.O., Mori, T., Finke, S., Conzelmann, K.-K., Young, J.A.T., and Callaway, E.M. (2007b). Monosynaptic restriction of transsynaptic tracing from single, genetically targeted neurons. Neuron *53*, 639–647.